Understanding Lithium-ion Dynamics in Single-ion and Salt-in-polymer Perfluoropolyethers and Polyethyleneglycol Electrolytes using Solid-state NMR

Chibueze V. Amanchukwu,[1,2,3,6]* Anna B. Gunnarsdóttir,[2,4,6] Snehashis Choudhury,[1] Tamsin L. Newlove,[2] Pieter C. M. M Magusin,[2,5] Zhenan Bao[1]*, and Clare P. Grey[2]*

1. Department of Chemical Engineering, Stanford University, Stanford CA 94305 USA
2. Department of Chemistry, University of Cambridge, Cambridge UK
3. Pritzker School of Molecular Engineering, University of Chicago, Chicago IL 60637 USA
4. Faculty of Industrial Engineering, Mechanical Engineering and Computer Science, University of Iceland, Reykjavík, Iceland
5. Present address: Institute for Life Sciences and Chemistry, HU University of Applied Sciences Utrecht, Netherlands
6. C.V.A. and A.B.G. contributed equally to this work.

*chibueze@uchicago.edu, *zbao@stanford.edu *cpg27@cam.ac.uk

Abstract

Lithium metal batteries with high energy densities can enable a revolution in energy storage and accelerate shifts in electric transportation and electricity generation. However, several morphological and electro-chemo-mechanical challenges impede their development. Solid state electrolytes such as those based on polymers show great promise in replacing liquid electrolytes in lithium metal batteries. Polyether-based polymer electrolytes are the most investigated but are plagued by low room temperature ionic conductivity and poor oxidative stability. Hence, there is a great need for the development and understanding of ion transport in new classes of polymer electrolytes. Perfluoropolyether (PFPE) based electrolytes have shown improved oxidative stability, but little is understood about their lithium solvation and transport mechanism. In this work, we use multinuclear solid-state magic angle spinning (MAS) nuclear magnetic resonance (NMR) spectroscopy to investigate the lithium cation environment and mobility in crosslinked single-ion and salt-in-polymer PFPE electrolytes and compare it directly to well-known polyethylene glycol (PEG) electrolytes. We show that the interaction of the lithium cation with the polymer backbone is weaker in PFPE systems compared to PEG, likely resulting in stronger ion pairing in the PFPE systems. Line shape analyses shows lower lithium mobility in PFPE electrolytes, despite lower activation energies being derived from spin-lattice relaxation (T_1) measurements as compared to those for the PEG systems. The rapid relaxation is instead ascribed to the local fluctuations caused by polymer backbone mobility. By studying different modes of ion binding (single-ion vs. salt-in-polymer), we show that differences across polymer backbones (PFPE vs PEG) have a greater effect on mobility than differences in ion binding modes within each polymer class (especially when single-ion conducting site density is not high). Our ability to use MAS NMR to study polymer electrolytes in their native state opens new opportunities to develop and understand novel polymer or hybrid solid state electrolytes for next generation lithium metal batteries.

Introduction

Developing batteries with higher energy densities is vital for electric transportation and a renewable-powered electric grid.[1] Replacing graphite anode (in current lithium-ion batteries) with lithium metal can at least double the overall battery gravimetric energy density.[2] Hence, there has been fervent research to develop rechargeable lithium metal batteries. However, prior efforts to commercialize rechargeable lithium metal batteries failed primarily because of the volatile, flammable liquid electrolytes, and the inability to prevent lithium dendrite growth upon metal deposition.[3] Designing solid state lithium metal batteries can alleviate these safety and morphological challenges, while maintaining high energy density.[3–5] Solid state electrolytes (SSEs) should support high ion conductivity ($> 10^{-3}$ S/cm), be mechanically flexible and thin (< 25 µm), and have a wide electrochemical stability window (0-4.5 V vs Li/Li$^+$).[3] Currently, inorganic SSEs such as phosphates (e.g., LATP), oxides (LLZO),[6] and sulfides[7] have been studied heavily.[3,4] Although inorganics such as sulfides have ion conductivities on the order of $10^{-2} - 10^{-3}$ S/cm,[8] no single class of inorganic electrolytes meets all the requirements.[9,10]

Polymer electrolytes are easy to process as a stand-alone SSE, as part of an inorganic-polymer hybrid electrolyte,[11,12] or as a binder for the cathode composite.[13,14] Furthermore, they can be mechanically flexible and fabricated in thin form factors. Polyethylene oxide or glycol (PEO/PEG) is the archetypal polymer electrolyte and has been studied for over four decades.[15–17] However, PEO still suffers from low room temperature ionic conductivity ($\sim 10^{-5}$ S/cm)[17] and poor oxidative stability (<4 V vs Li/Li$^+$)[18], preventing its use either as a stand-alone SSE or as part of a cathode composite where voltages cutoffs typically exceed 4 V_{Li} (e.g., with LiCoO$_2$, LiNi$_x$Mn$_y$Co$_z$O$_2$). The oxidative challenges facing PEO also plague small ether molecules.[19] New polymer backbone chemistries that do not require the ether group for ion conduction are needed. Polycarbonates such as polyethylene carbonate have been explored, but still suffer from low room temperature ionic conductivity and poor oxidative stability.[20–22]

Recently, we synthesized a new class of fluorinated-ether small-molecule-electrolytes that show high ionic conductivity and high oxidative stability.[23–25] This finding prompted us to explore solid perfluoropolyether (PFPE) as a polymer electrolyte. While polycarbonates have been extensively studied,[20–22,26] there has been limited work on solid PFPE.[18,27] Previous work[27] has shown that crosslinked PFPE can support ion transport, albeit still with low conductivities ($\sim 10^{-5}$ S/cm). And previous solution state work done by some of us[23] and Balsara and coworkers[28,29] have shown higher lithium transference number in the perfluoroether backbone indicating weaker lithium coordination of the polymer backbone compared to the traditional PEG. In addition, Lee et al.[18] used density functional theory to show that PFPE has a higher oxidation potential and a higher electrochemical stability window compared to PEO, which was also observed experimentally in small molecule perfluoroether electrolytes.[23–25] However, little is known about the lithium ion solvation structure, mobility, and transport mechanism in solid PFPE electrolytes.

There are two classes of polymer electrolytes with different ion transport mechanisms: 'single-ion'/polyelectrolyte and 'salt-in-polymer' (see Figure 1a). Salt-in-polymer electrolytes involve a lithium salt dissolved in a polymer and usually suffer from low lithium transference numbers (with higher mobility of the anion compared to the cation under an electric field).[13] To improve the transference number, single-ion/polyelectrolytes have been developed that immobilize the salt anion within the polymer backbone making the lithium ion the only mobile species, leading to a lithium transference number close to unity.[30,31]

In this work, we fabricated single-ion and salt-in-polymer PFPE, with the tethered TFSI anion and LiTFSI salt dissolved (Figure 1), respectively. Magic angle spinning (MAS) NMR was used to study polymer environment, the lithium ion solvation structure and activation barrier for ion transport.[32] MAS NMR provides high chemical shift resolution for these solid polymers and enables an understanding of ion

solvation and mobility in their natural solid-state, without need to dissolve the polymers in solvents.[33–35] Lithium (^{7}Li) NMR was used to study the cation, while fluorine (^{19}F) and proton (^{1}H) NMR was used to characterize the anion and polymer backbone behavior.

We perform equivalent analyses on single-ion PEG and salt-in-polymer PEG to provide insight into the differences between the two classes of polymer backbone. We find that lithium interacts more weakly with the PFPE backbone as compared to PEG, and the lithium ion mobility in PFPE is less strongly coupled to the polymer mobility as compared to PEG. The lithium ion mobility is strongly temperature dependent in PEG whereas only minor effects are observed in PFPE. Finally, the activation energy for lithium mobility was estimated by spin-lattice relaxation (T_1) measurements and reveals a lower energy barrier in the salt-in-polymer PFPE-system compared to PEG, likely due to the rapid motion of the polymer backbone. Insights gained from the use of MAS NMR regarding the ion transport behavior will enable the development of next generation ion conducting polymer electrolytes.

Results and Discussion

Synthesis and physicochemical characterization

The 'single-ion' and the 'salt-in-polymer' electrolytes were synthesized according to previously published procedures.[27,31] The electrolytes were crosslinked to obtain mechanically compliant, stand-alone films. Since all the precursors for the single-ion polymer are soluble in tetrahydrofuran (THF), and the monomer precursors for the 'salt-in-polymer' are liquid, crosslinking leads to insoluble solids (visual confirmation). Figure 1 shows the structures of the polymer precursors and a schematic for the subsequently crosslinked structure. For the single-ion conductor, the TFSI anion was tethered to the backbone using the thiol functionality (Figure 1b). Three different concentrations of the single-ion PFPE were studied: S0 (0 wt% TFSI tethered), S5 (5 wt% TFSI tethered), and S15 (15 wt% TFSI tethered). Note, these are the nominal values, because not all the added TFSI will crosslink within the chain (see Experimental Section for more detailed discussion). By changing the PFPE to a PEG, we can make direct comparisons between a single-ion PFPE (PFPE-S0, S5, S15) and a single-ion PEG (PEG-S15).

The 'salt-in-polymer' electrolytes were prepared by completely dissolving 20 wt% LiTFSI in the monomers (PEG-diacrylate and PFPE-methacrylate) and photo-crosslinking to obtain solid polymer electrolytes. 20 wt% LiTFSI in PEG corresponds to an EO/Li ratio of 1.6 and O/Li ratio of 6.6 while 20 wt% LiTFSI in PFPE corresponds to an EO/Li ratio of 1.5 and O/Li of 5.3 (Table S1). These polymers are conventional in the sense that both cation and anion are expected to be mobile in the crosslinked matrix. By comparing the salt-in-polymer PFPE to PEG, we can draw insights from previously explored crosslinked PEG systems.[34,36]
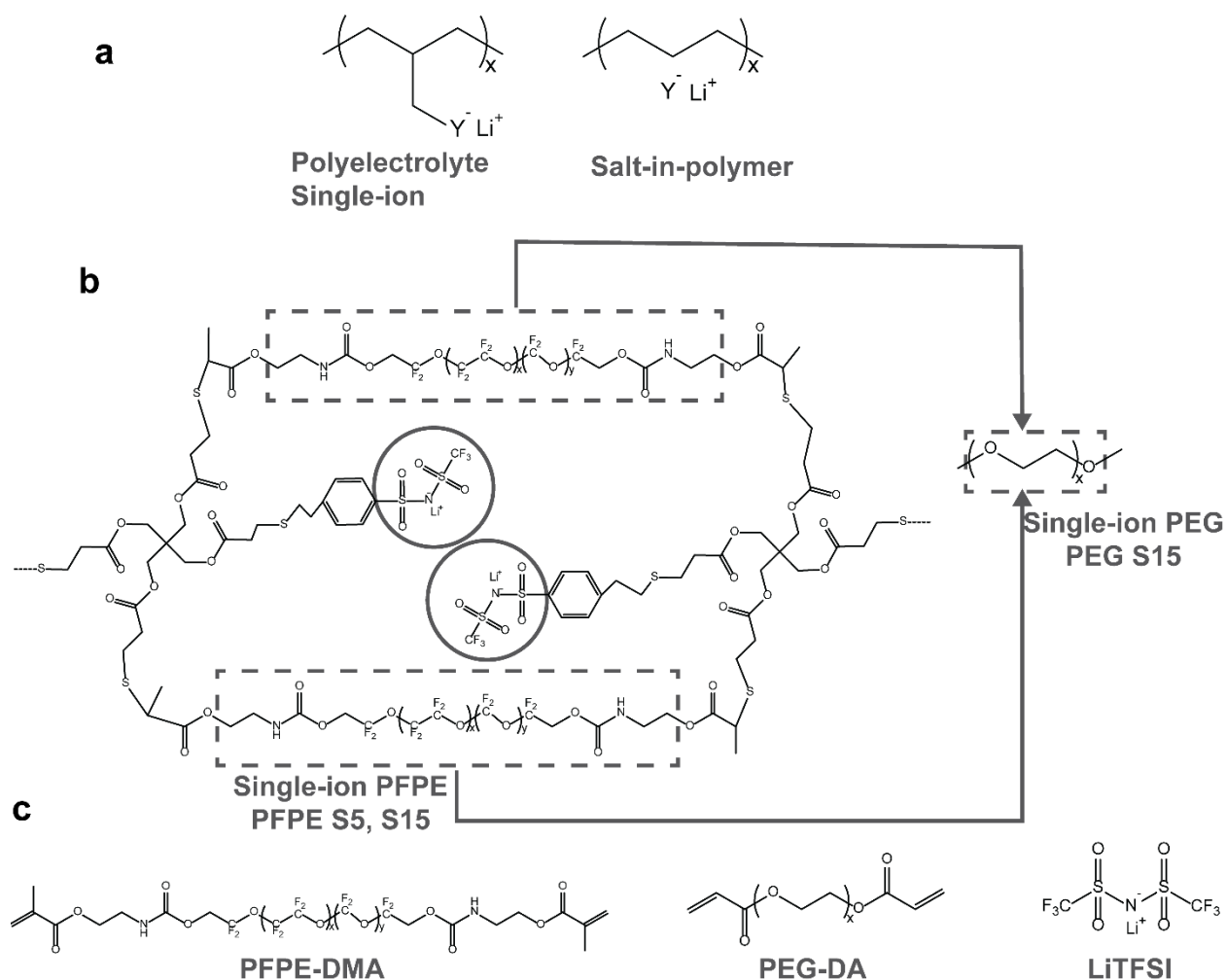
Figure 1 | Schematic of polymer electrolytes. (**a**) Illustration of the difference between a polyelectrolyte/single-ion and a 'salt-in-polymer' polymer electrolyte. (**b**) Schematic of a crosslinked single-ion PFPE. S5 and S15 correspond to the percentage of TFSI (5 or 15 wt%) attached to the polymer chain (circled in **b**), and the "S" indicates it is a single-ion polymer. When the PFPE repeat units in the dashed boxes are replaced by the PEG repeat unit as showcased by the arrows, the single-ion PEG is obtained (PEG-S15). (**c**) Chemical structures for PFPE-DMA, PEG-DA, and LiTFSI. These are used to fabricate 'salt-in-polymer' by dissolving 20 wt% LiTFSI salt in the liquid monomer (either PFPE-DMA or PEG-DA) and photo-crosslinking. Chemical structure of PFPE-DMA obtained from Devaux et al.[27]

MAS NMR and Fourier Transform infrared (FTIR) spectroscopies were used to confirm the PFPE polymer structures (Figures S1-S4). FTIR data in Figure S4 shows the incorporation of the TFSI in the single-ion polymers with peak at 1625 cm^{-1}, which is present in both PFPE-S5 and PFPE-S15 but is absent in PFPE-S0. In addition, the sets of peaks from $610 - 540$ cm^{-1}, associated with a SO$_2$ scissoring vibration from TFSI are present in both PFPE-S5 and S15, but not in PFPE-S0. For the salt-in-polymer, these sets of peaks are also observed indicating the presence of LiTFSI. The combination of visual (liquid to solid), FTIR (Figure S4), and solid-state NMR provided evidence of crosslinking in these polymer electrolytes and engendered probing of thermal behavior and ion mobility.

The thermal properties of the polymer electrolytes were studied using thermogravimetric analysis (TGA) and differential scanning calorimetry (DSC). The TGA data in Figure S5 shows that the polymer electrolytes are stable until at least 250°C. The DSC data in Figure S6 shows that PFPE-S0 and PFPE-S15 have a weak T_g around –18°C, higher than the T_g of pure PFPE that is typically around –90°C,[27,37] and may be due to the crosslinking sites. However, 20 wt% LiTFSI in PFPE does not show a glass transition, an observation similar to that reported by Balsara et al.[27] Meanwhile, there are no glass or melting transitions for PEG-S15 and 20 wt% LiTFSI in PEG in the temperature range studied (–50 to 120°C). Work by Schönhoff et al.[33] show a T_g of –45°C for crosslinked PEG with no salt and a T_g of –32°C with 30 mol% LiTFSI. It is possible that the lower –50°C DSC temperature cutoff (T_g could be lower) or different sample preparation techniques contribute to the absence of a T_g in our crosslinked PEG samples.

Polymer-backbone environments and dynamics

The temperature dependence of the polymer backbone was studied using ^{1}H NMR and ^{19}F MAS NMR spectroscopy. Within amorphous polymer electrolytes, polymer segmental motion is required for ion transport and thus the ion mobility is often coupled to mobility of the backbone.[17,38] Hence, comparing the environments within the different polymer classes is vital.

Figure 2a shows the ^{19}F MAS NMR spectra of the solid PFPE-S15 polymer as a function of temperature. The main resonances correspond to $(-CF_2CF_2O-)_x$ units in the polymer backbone around -89 to -91 ppm and the $(-CF_2O-)_y$ units around -52 to -56 ppm. Table S2 summarizes the chemical shifts for the different groups of the polymer backbone.[37,39] Integration of the resonances for $(-CF_2CF_2O-)_x$ and $(-CF_2O-)_y$ (see Figure 1b) results in a ratio of $x/y \approx 7/3$, consistent with previous reports.[37]

Interestingly, the fluorinated PFPE polymer groups give rise to sharp resonances whereas the resonance of the TFSI anion (Figure S2, expected at around -81 ppm)[37] is broad indicating a mobile fluorinated polymer backbone and a more constrained TFSI anion (potentially including LiTFSI aggregates). The TFSI group is not directly observed in PFPE-S15 even though ^{7}Li MAS NMR in Figure S2 shows the presence of lithium (hence, an anion must be present) in PFPE-S15. Integration of the ^{19}F spectra shows that the TFSI peak is buried underneath the strong signal of the PFPE backbone (Table S2). The absence of the TFSI peak could also be due to broadening from [19]F-^{19}F homonuclear dipolar coupling as seen when comparing the TFSI resonance in PFPE and PEG polymer electrolytes (Figure S3), and also the rapid motion in this system affecting the ability of MAS to effectively remove the [19]F-^{19}F homonuclear coupling (see discussion for [7]Li below). The resonance of TFSI is narrow in PEG polymer electrolytes compared to PFPE (consistent with previous reports),[37] possibly due to weaker ^{19}F homonuclear dipolar coupling.

The resonances of the $-CF_2CF_2O-$ and $-CF_2O-$ units do not shift with salt addition (shown in Figure S7), suggesting the polymer backbone is weakly affected by the addition of lithium ions. The backbone resonances shift only slightly with temperature and the line width remains constant within the temperature regime studied (Figures 2a and 2c). The lack of sensitivity to temperature and the observation of extremely sharp resonances in a system with strongly coupled ^{19}F spin-systems (CF_2 groups) at the relatively slow MAS frequency of 8 kHz indicates that the PFPE polymer chains are already in the NMR fast motion regime and highly mobile even at -20°C.
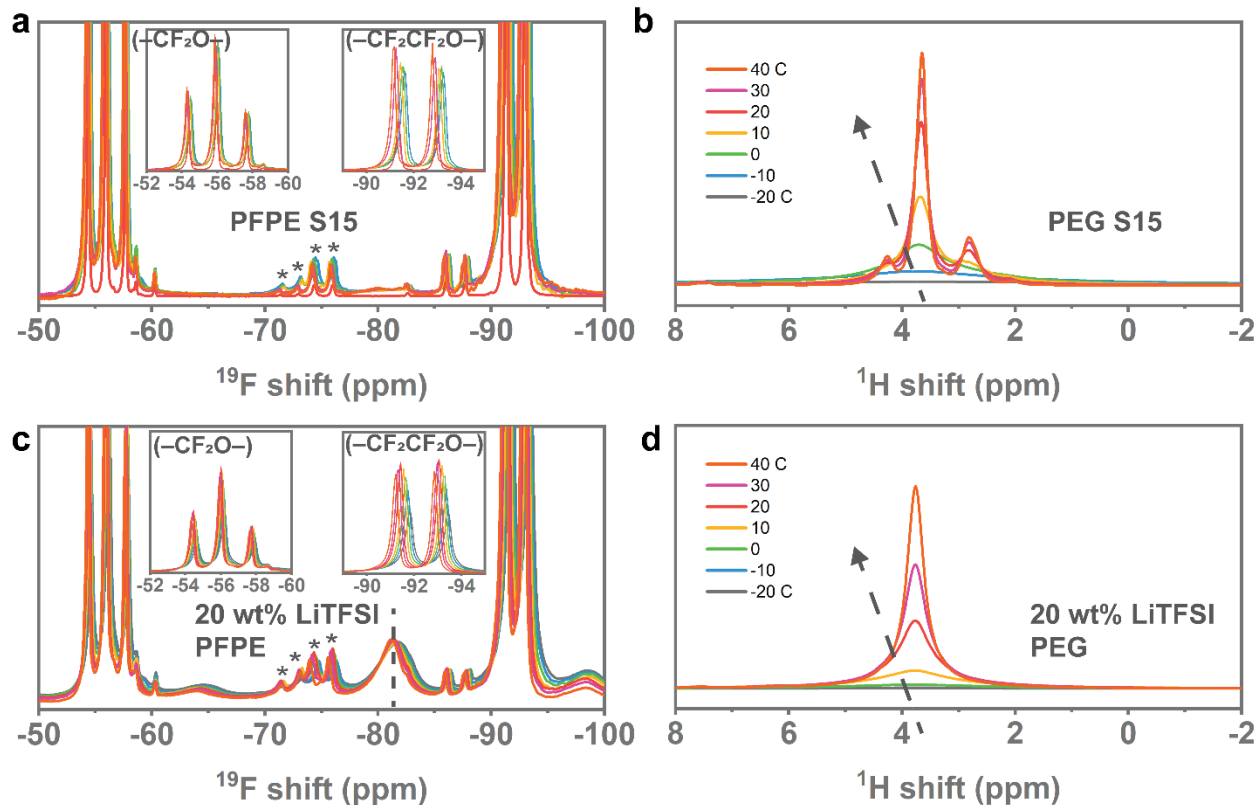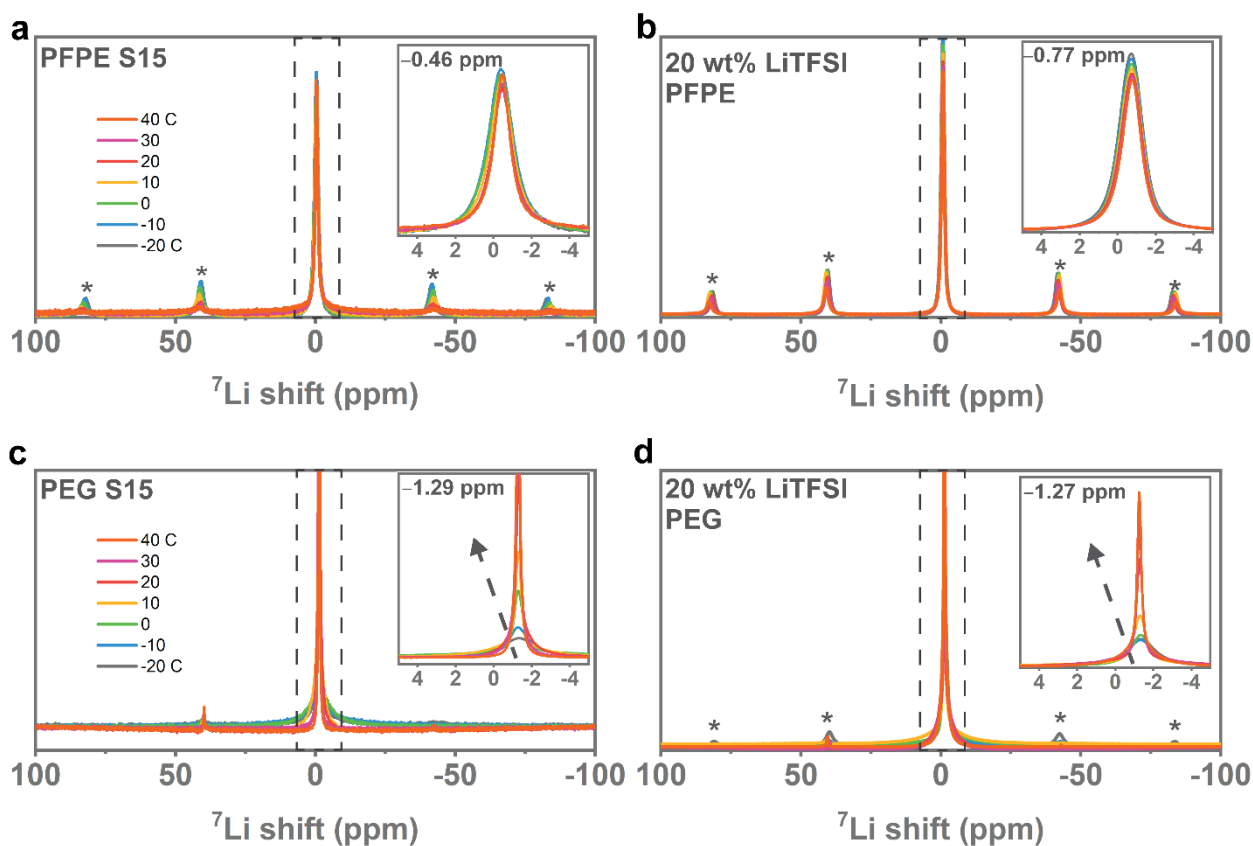
Figure 2 | Polymer environment as a function of temperature. ^{19}F MAS NMR (rotor-synchronized Hahn echo) spectra as a function of temperature for (**a**) PFPE-S15 and (**c**) 20 wt% LiTFSI in PFPE. The insets in both figures are magnified sections showing the truncated regions of the full spectra. The vertical dashed line in (c) indicates the TFSI chemical shift (–81.3 ppm). ^{1}H MAS NMR spectra as a function of temperature for (**b**) PEG-S15, and (**d**) 20 wt% LiTFSI in PEG. The slanting arrow in (b) and (d) indicates the direction of change with increasing temperature. A temperature range from –20 to 40°C with a 10°C increment was studied. Temperature color scale in (b) and (d) are the same for (a) and (c). Spinning sidebands are denoted by asterisk (*). MAS spinning speed: 8 kHz.

Figures 2b and 2d show the ^{1}H NMR spectra for the PEG polymer electrolytes, where the resonances are broad at -20 °C and narrow significantly with temperature, indicating increasing mobility of the backbone. In addition, the ^{1}H peak for the salt-in-polymer 20 wt% LiTFSI in PEG shifts downfield (3.77 ppm) compared to PEG S15 (3.65 ppm) at 30°C. Both single-ion PFPE and PFPE salt-in-polymer were crosslinked using CH_2-methacrylate groups, hence the ^{1}H NMR signals in PFPE (Figure S8), which show some temperature sensitivity. The differences between the polymer backbone (PFPE vs PEG) as a function of temperature significantly outweigh the differences between ion coordination environment (single-ion/polyelectrolyte vs salt-in-polymer) within the same polymer class.

Lithium-ion environment and dynamics

Figure 3 shows the ^{7}Li MAS NMR spectra, which were used to study the lithium-ion environment in the single-ion and salt-in-polymer electrolytes as a function of temperature. In both systems, the lithium cations

will coordinate to the negatively charged TFSI anions or to the tethered anion backbone of the single-ion polymer and thus the coordination environments and mobility are likely to differ. [7]Li is a quadrupolar nucleus (I = 3/2) and here all polymer electrolytes show a single [7]Li peak that consists of a narrow component due to the (-1/2 ↔ 1/2) central transition and a broader component, or a quadrupolar component, associated with the satellite transitions (± 3/2 ↔ ± 1/2) (the line shape shown in more detail in Figures S10 and S11) that results in spinning sidebands under MAS.[40,41] For the PEG polymers (Figures 3c-d), a broad line shape is observed at the lower temperatures which sharpens significantly as the temperature is increased, consistent with the behavior of the polymer backbone. For the PFPE polymers, there are minimal changes to the central peak with temperature, mirroring the behavior of the backbone as observed in Figure 2. The intensities and widths of the [7]Li spinning sidebands do, however, change noticeably with temperature, indicating motion.

Figure 3 | Lithium-ion local environment as a function of temperature. ^{7}Li MAS NMR spectra as a function of temperature for (**a**) PFPE-S15, (**b**) 20 wt% LiTFSI in PFPE, (**c**) PEG-S15, and (**d**) 20 wt% LiTFSI in PEG. The dashed box in figures (a-d) corresponds to the inset. The chemical shift values indicated in the inset corresponds to the maximum peak at 30°C. The arrow indicates increasing temperature. Temperature range from –20 to 40°C with a 10°C increment. The temperature color scales in (a) and (c) are the same for (b) and (d). Spinning sidebands are denoted by asterisks (*). MAS spinning speed: 8 kHz.

The line width of the central peak was first quantified to probe lithium mobility, where line narrowing is expected with increasing temperature due to motional averaging of dipolar (and to a lesser extent for [7]Li)

quadrupolar interactions.[34,35] Figure 4a shows a decrease of around 30% in line width for both PFPE-S5 and S15 as the temperature increases between -20 and 40 °C compared to only 19% in the salt-in-polymer PFPE, indicating poorer ion mobility in the salt-in-polymer. In contrast, a sharp decrease in line width of around 85% is observed for both PEG-S15 and 20 wt% LiTFSI in PEG. The significant changes in line width for PEG-S15 may not be attributed to thermal transitions alone, as the DSC data in Figure S6 shows no thermal transitions between –20 to 40°C, and are consistent with higher Li$^+$ mobility.
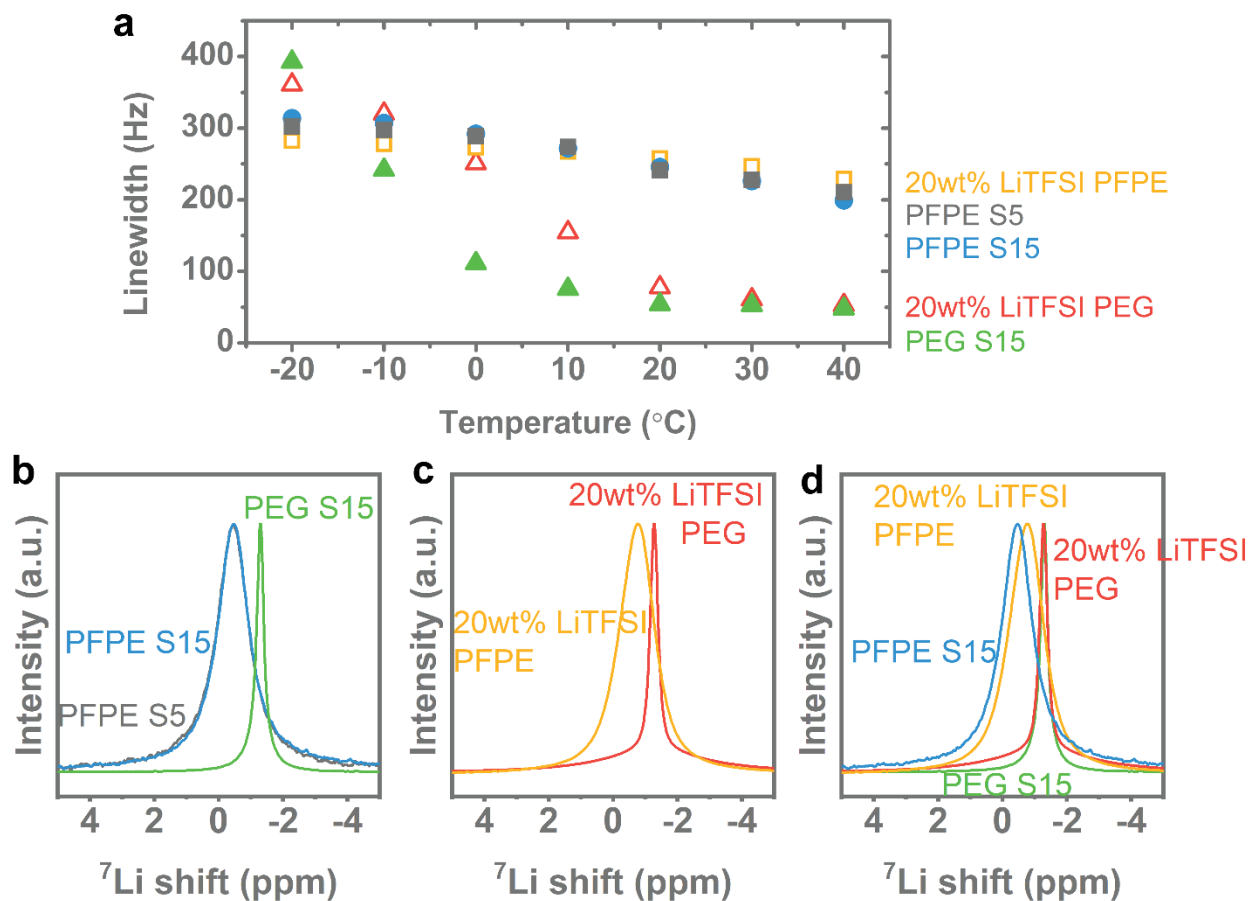
Figure 4 | Lithium-ion local environment as a function of temperature. **a**) ^{7}Li full width half maximum (FWHM) of the central transition (i.e. isotropic resonance) as a function of temperature for all the polymers. ^{7}Li MAS NMR spectra at 30°C of **b**) PFPE-S5, PFPE-S15 and PEG-S15; (**c**) 20 wt% LiTFSI in PFPE and PEG; (**d**) PFPE-S15, PEG-S15, 20 wt% LiTFSI in PFPE and PEG. Peaks normalized to the peak of highest intensity. (a.u.) = arbitrary units.

Motional effects can also be observed via the spinning sideband manifold (Figure 3), where a loss of intensity is due to motional averaging of anisotropic interactions. For both PEG electrolytes the satellite transitions collapse into the central transition with increased temperature, which we mainly attribute to averaging of the quadrupolar interaction. However, in contrast to PEG-S15, a noticeable broadening and then sharpening of the spinning sidebands manifold is seen for 20wt% LiTFSI PEG (see Figure S12).

To gain more insight into motional effects of the quadrupolar interaction, deconvolutions of the NMR spectra were performed using the dmfit software package.[42] The spinning sideband manifold is captured by the broad component, attributed to the satellite transitions. The line widths of the central and satellite peaks

from the spectral fittings and the extracted values of the quadrupolar coupling constant Q_{cc} are summarized in Figures S12 and S13 over the measured temperature range.

In 20wt% LiTFSI PEG, an initial broadening is seen for the satellite line width, the satellites then narrowing at temperatures above 0°C. This broadening is a clear indication of slow motion.[43–46] In the limit where the MAS frequency is greater than the quadrupolar coupling, maximum broadening occurs for motion on the order of the spinning frequency (here 8 kHz); when the MAS frequency is less than the static quadrupolar coupling constant, the hopping rate at which maximum broadening occurs is higher than the MAS frequency and now also depends on the quadrupolar frequency. However, for the quadrupolar coupling constants derived for this system (see SI) the maximum broadening is seen for hop rates of a similar order of magnitude. Thus, for 20wt% LiTFSI PEG, the motional broadening indicates motion occurring on the $\sim 10^{-4}$ s timescale.[46] In contrast, PEG-S15 shows negligible spinning sidebands intensity, indicating that the quadrupolar interaction is effectively being averaged over the whole temperature range, also shown with continuous decrease in line width of the broad component that is present under the sharper central transition peak. This indicates higher lithium-ion mobility in PEG-S15 that is already faster than the MAS frequency (8 kHz) at -20°C. For PFPE-S15 the spinning sideband intensity decreases with temperature and is mirrored in an increase in line width of the broad component (see Figure S12). In comparison, the cations in 20wt% LiTFSI in PFPE show no onset of motion, with little differences seen in the line widths over the whole temperature range (Figure S12). In conclusion, line shape analysis with temperature suggests that the lithium ions in the single-ion polymer electrolytes have greater mobility as compared to the salt-in-polymers within each polymer class.

The influence of salt concentration within the single-ion PFPE electrolytes was also studied and Figure 4b shows that as the salt concentration is increased from PFPE-S5 to PFPE-S15, the [7]Li chemical shift remains constant at –0.46 ppm, indicating little change in the lithium ion environment. An upfield shift (negative shift) to –0.7 ppm is observed in 20 wt% LiTFSI in PFPE, indicating different chemical environments to the single-ion polymer, possibly due to formation of ion aggregates. As Figure 4d shows, the chemical shifts for both PEG-S15 and 20 wt% LiTFSI in PEG overlap and are further upfield compared to the PFPE electrolytes (at –1.29 ppm), consistent with significant ether-Li binding,[17,41,47] and/or interactions with the TFSI units due to ion pairing. The chemical shift reported for pure LiTFSI salt (using LiCl at 0 ppm as a [7]Li reference) is –1.2 ppm.[12]

The downfield chemical shift observed in the PFPE indicates that it cannot be solely bound to multiple TFSI units (as in the salt LiTFSI). However, the lack of an observable change of the polymer backbone in the ^{19}F spectrum between the single-ion and salt-in-polymer systems suggests that the backbone interacts only very weakly/if at all with the Li^+ ions (Figure S7). The higher frequency shift of Li^+ ions in PFPE compared to PEG is thus ascribed to a lower coordination environment (small number of ligands) for Li^+ or possibly the interaction with other ligands such as the methacrylate groups. The fluoroether backbone is known for its low polarity and has seen significant use as chemically resistant oils.[48]

^{19}F MAS NMR of the TFSI anion (Figure S9) shows similar temperature dependence as the lithium ion in Figure 3. In PEG there is significant decrease in line width of the TFSI; in 20 wt% LiTFSI PEG the TFSI appears upfield (–79.7 ppm) compared to PEG S15 (–78.6 ppm) at 30°C, which may indicate stronger ion pair formation for the salt-in-polymer. However, the TFSI peak in both PEG polymers are both downfield compared to the TFSI peak in 20 wt% LiTFSI in PFPE (–81.3 ppm). In conclusion, for both PEG and PFPE electrolytes the temperature dependence of the lithium and anion peak mirrors the polymer behavior,

indicating that polymer and ion chemical environments are intertwined and will have implications for ion transport.

Relaxation behavior and activation energy

The dependence of the spin-lattice (T_1) relaxation with temperature is a sensitive probe of motion on the order of the Larmor frequency ($\sim 10^{-9}$ s). ^{7}Li can undergo relaxation via both dipole-dipole and quadrupolar mechanisms where the quadrupolar interaction is expected to be dominant in these polymer systems.[34,35,49] The relaxation times for ^{7}Li are shown in Figure 5 and are shorter in the PEG polymer system compared to the PFPE. Shorter T_1 times for the PEG are consistent with faster lithium ion mobility and possibly a different ion transport mechanism. For the temperature range studied (–20 to 40°C), no T_1 minima were recorded, making it difficult to use the Bloembergen-Purcell-Pound (BPP) equation and extract correlation times.[34,36] Instead a single-exponential fit was used to extract the effective activation energy barriers assuming the $1/T_1$ rates follow an Arrhenius law given by $1/T_1 \propto \exp\left(-\frac{E_a}{k_B T}\right)$. The activation energies are summarized in Figure 5b. The nonlinear nature of the PEG-S15 data made for a poor Arrhenius fit (Figure 5a) – instead there appears to be weak T_1 minimum at approximately 270 K superimposed on a second T_1 process.

The single-ion PFPE polymers have a higher activation energy barrier for Li$^+$ mobility compared to the salt-in-polymer, and increase with higher salt content, 15 kJ/mol and 18 kJ/mol for PFPE-S5 and S15 respectively. The activation energy for 20 wt% LiTFSI in PFPE (9 kJ/mol) is similar to the value (~ 9.5 kJ/mol) obtained previously from conductivity measurements of a PFPE liquid electrolyte.[27] In comparison, the salt-in-polymer 20 wt% LiTFSI PEG gave an activation energy of 26 kJ/mol (O/Li = 6.6), which is similar to other reported NMR obtained activation barriers for LiCF$_3$SO$_3$ in PEO (24 kJ/mol, O/Li = 8),[40] and LiBF$_4$ and LiClO$_4$ in PEG (24 kJ/mol).[50] This is consistent with the work of Balsara and coworkers that has shown that the activation barrier for ion transport in liquid PFPE is lower than that obtained in liquid PEG.[37]

Despite the lack of T_1 minima, an attempt was made to use the BPP model (see discussion in the SI and Figure S14) to estimate the order of magnitude for the lithium correlation times (τ_c). Similar activation energies were obtained using the simple Arrhenius fit and the BPP model, giving some confidence in the fitting (Table S3). The calculated correlation times in the PFPE polymer systems (Figure S15-S16) are four times longer than in the PEG system at room temperature, consistent with reports of lower conductivity in PFPE electrolytes.[37] Others have reported that the Arrhenius preexponential factor – a proxy for number of charge carriers – is three orders of magnitude lower in liquid PFPE than PEG.[37]
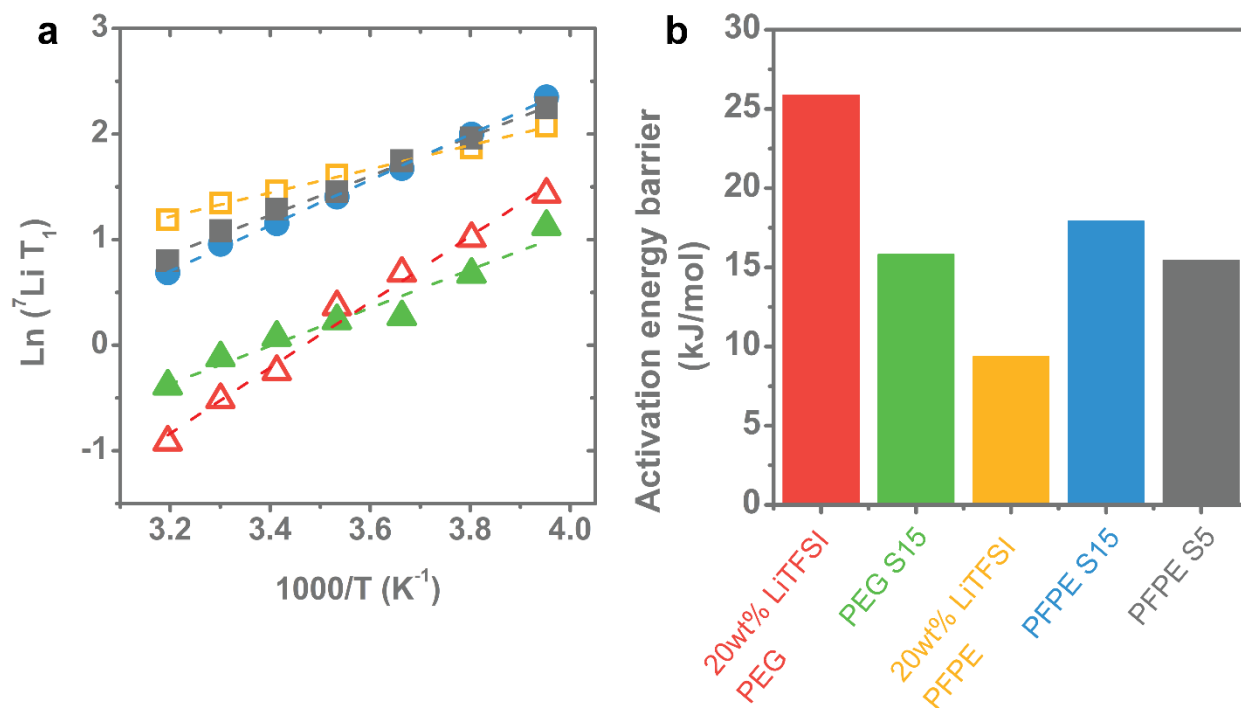
Figure 5 | Ionic motion and relaxation behavior. (**a**) ^{7}Li spin-lattice relaxation times (T_1) as a function of temperature. Lines shown are linear fits. (**b**) the activation energies obtained from Arrhenius fit to the T_1 data in (a). The labeling color scheme in (b) is the same as in (a).

Consequences for lithium ion transport

In PEG-based polymer electrolytes, lithium ions coordinate with the polymer, and segmental motion of the polymer enables lithium-ion transport.[17] Here, the PFPE backbone is highly mobile at all temperatures studied (on the basis of the ^{19}F NMR in Figure 2). Furthermore, no significant change in the ^{19}F chemical shifts in the PFPE backbone are seen with salt addition (Figure S7), indicating that the lithium ion interacts weakly with the PFPE polymer backbone. Unlike the ether oxygen in PEG, the fluorine atoms in PFPE will withdraw electron density from the fluoroether oxygens, limiting their ability to bind lithium ions strongly. Note that PFPE electrolytes have both fluoroether oxygen atoms as well as the methacrylate group, but the PFPE alone (without any hydrogenated end groups) does not dissolve salt as we have seen through our own experiments. In contrast, the ether group in PEG has been reported to solvate and support ion transport, regardless of the end group selection.[17] Thus, much stronger Li^{+}-TFSI^{-} ion pairing likely occurs in the PFPE systems, the Li ions binding more strongly to the negatively charged TFSI groups, the TFSI groups acting as local traps. The weak interactions between the PFPE and Li^{+} ions contribute to the lower conductivity of the PFPE vs. PEG-based systems – despite the high mobility of the PFPE backbone.

Low Li^{+} mobility is observed for PFPE-S15, even lower mobility being seen (on the basis of the ^{7}Li sideband manifolds) for the salt-in-polymer. The low Li mobility is consistent with long range measurements of Li transport (conduction), which are lower for the PFPE vs PEG systems.[37] Our studies of PEG systems by contrast show gradually increasing motion of the PEG backbone with temperature, rapid Li mobility being seen at higher temperatures. Yet the 20 wt% LiTFSI in PFPE has the lowest activation barrier for Li^{+} motion measured in this work.

Higher activation energy barriers were calculated for the single-ion PFPE compared to salt-in-polymer PFPE (Figure 5) despite the faster ion mobility observed through line shape analyses. The activation barriers determined by the NMR relaxation measurements are unlikely, however, to be directly related to long-range translational motion. In support of this, the Li^+ line shape analysis suggested that Li mobility was in the kHz timescale (correlation times of the order or 10^{-4} s) while the relaxation analysis suggested correlation times of the order of 10^{-8} s (Figure S15). Thus, the dominant relaxation mechanisms must arise from short-range dipolar and quadrupolar interactions, the high mobility of the PFPE polymer chains likely driving the relaxation of the Li cation, not the Li mobility. Even though Li binding to the chains is weak, the overall mobility of the backbone will result in high frequency fluctuations of the whole system.

With NMR sensitive to localized motion on short time scales, efforts were made to compare the activation energies obtained from T_1 measurements to pulsed field gradient (PFG)-NMR diffusion measurements. However, due to the extremely short T_2 relaxation time (on the order of 0.1 ms), the diffusion coefficient of the cation could not be measured. However, our results compare well with reported conductivity measurements; the line shape analysis shows the ion motion is much faster in the PEG systems that corroborates with higher ionic conductivity data reported for PEG systems[17] and low activation energy for Li conduction has been reported for the PFPE system.[27]

The interest in PFPE systems is due to their increased oxidative stability as predicted by DFT.[18] However, our work shows that the PFPE backbone suffers from poor ionic solvation, which is responsible for the lower ionic conductivity observed in crosslinked PFPE.[27] An approach to improve ionic solvation in fluorinated electrolytes was recently explored in a new class of small molecule electrolyte that eschew the fluoroether oxygen within the polymer backbone,[24] and another approach that adds ether groups to the PFPE 'end-group' to get combined improved ion solvation/transport coupled to desired high electrochemical stability.[23] These approaches may lead to improved polymer-ion interactions within the PFPE polymer class and enable a next generation of highly conductive PFPE electrolytes.

Conclusions

The lack of ionically conducting, electrochemically and mechanically stable solid-state electrolytes has hampered the development of lithium metal batteries. Ether-based polymer electrolytes have been heavily studied but suffer from low room temperature ionic conductivity and poor oxidative stability. In contrast, PFPE-based electrolytes are purported to have higher oxidative stability, although little is understood about lithium ion solvation and transport in solid-state PFPE electrolytes. In this work, we use ^1H, ^7Li, and ^{19}F MAS NMR to study PFPE and PEG based polymer electrolytes and show that while the polymer back-bone mobility of PFPE is extremely rapid and even liquid-like at room temperature, only slow Li motion (on the kHz timescale) is observed. By contrast, the motion of the PEG backbone increases gradually with temperature in the relevant battery temperature range –20 to 40°C, this motion tracking an increase in Li^+ mobility. The ^7Li and ^{19}F chemical shift data shows that the lithium ion interacts weakly with PFPE compared with PEG, suggesting that the Li ions are instead bound more strongly to the negatively charged TFSI groups, either on the polymer or introduced as salts. More ion pairing likely exists in the PFPE systems than in the PEG systems where the Li^+ ions are more effectively dissociated from the negative counter anions (or charge) by binding to the ether groups.

The activation energy barrier obtained using NMR relaxation measurements mirrors that obtained in literature from conductivity measurements and is lower for the PFPE electrolyte compared to PEG. However, the rapid relaxation times observed by NMR in the PFPE system are associated instead with the

mobility of the PFPE chains as opposed to the long-range transport of the Li^+ ions. Despite the stronger ether-Li binding in crosslinked PEG, quantification of the ^7Li NMR line shapes shows that ion motion is faster in PEG compared to the PFPE electrolytes. By contrasting single-ion/polyelectrolytes with 'salt-in-polymer,' our work indicates that ion mobility increases in single-ion/polyelectrolytes for both crosslinked PEG and PFPE, but that the identity of the polymer backbone (PEG vs PFPE) has a stronger influence on ion solvation and mobility. Using MAS NMR to study these polymer electrolytes in their native solid state will allow us to translate these insights into the design of next generation non-ether polymer electrolytes for lithium-based batteries.

Acknowledgements

Experimental Details

Materials and Synthesis:

Poly(ethylene glycol) diacrylate (PEGDA; M_n=700) was obtained from Sigma-Aldrich. Per(fluoropolyether) dimethacrylate (PFPE DMA; M_w = 1500) is a bifunctional urethane-methacrylate and was obtained from Cornerstone company (Fluorolink MD700). Pentaerythritol tetrakis(3-mercaptopropionate) ("Tetrathiol") and 2,2-dimethoxy-2-phenylacetophenone (DMPA) were obtained from Sigma-Aldrich. Tetrahydrofuran was obtained from Fisher Scientific. LiTFSI was obtained from Solvionic.

'Single-ion' conducting polymers

Lithium 4-styrenesulphonyl(trifluoromethylsulphonyl) imide (STFSI Li) was synthesized according to a procedure previously reported.[31,51] To obtain PFPE-S5, S15, and S50: STFSI Li was mixed with tetra-thiol crosslinker, PFPE, and DMPA initiator. (wrt) = "with respect to"

PFPE-S0 [0 wt% STFSI, 5 wt% of DMPA initiator with respect to (wrt) PFPE + STFSI]

PFPE-S5 [5 wt% STFSI wrt PFPE DMA, 1:1 mole ratio (-SH:STFSI+DMA); 5 wt% DMPA]

Example: 1 g PFPE DMA; 0.05 g STFSI; 0.182 g tetrathiol; 0.052 g DMPA]

PFPE-S15 [15 wt% STFSI wrt PFPE DMA, 1:1 mole ratio (-SH:STFSI+DMA); 5 wt% DMPA]

PFPE S50 [50 wt% STFSI wrt PFPE DMA, 1:1 mole ratio (-SH:STFSI+DMA); 5 wt% DMPA]

PEG-S15 [15 wt% STFSI wrt PEGDA, 5wt% DMPA initiator wrt PEGDA + STFSI]

These components were added to a vial and tetrahydrofuran (THF) was added and stirred to dissolve the components. However, for the mixtures containing STFSI, not all STFSI dissolved. Hence, the STFSI ratio reported are nominal values, and the actual STFSI content in the crosslinked network will be lower. The solution was then exposed to ultraviolet light (handheld, 365 nm) for crosslinking. For PFPE-S0 and S5, crosslinking happened even before exposure to UV. For the PFPE S50, a 400W lamp was used for 35 minutes to induce crosslinking. Once crosslinking occurred for all the polymer samples, they were washed copiously (at least three times) with excess THF. The polymers were then placed in a 60°C overnight to dry.

'Salt-in-polymer' conducting polymers

PFPE DMA and PEGDA were vacuum dried at 100°C before transfer to an Argon glovebox. In an Argon-filled glovebox (MBraun, O_2 < 0.1ppm, H_2O < 0.1ppm), the following measurements were made. In a 20 mL vial, 3 grams of PFPE DMA was added, followed by 0.75 grams of LiTFSI (to obtain 20 wt%). The vial was stirred at 90°C to fully dissolve the salt. Then, 30 mg DMPA was added and stirred until dissolution. As soon as DMPA dissolved, the contents were poured into a Teflon dish and irradiated with a handheld UV lamp (365 nm) for 3 minutes. The film could be easily peeled off from the dish.

For 20 wt% LiTFSI in PEGDA, a similar procedure was followed. Here, 2 g of PEGDA, 0.5 g LiTFSI, and 20 mg DMPA. The contents were poured into a glass dish, and crosslinked with a handheld UV lamp (365 nm) for 3 minutes.

Characterization (FTIR, TGA, DSC): FTIR characterization was performed in an Argon-filled glovebox (MBraun, O_2 < 0.1ppm, H_2O < 0.1ppm) with an Agilent Cary 630 spectrometer. TGA characterization was performed using a Mettler Toledo/DSC 2. A 10°C/min scan range was used from 30°C to 500°C under a nitrogen environment. DSC characterization was performed using a Perkin Elmer DSC 4000. DSC procedure: (1) Hold at 30°C for 2 minutes. (2) A 20°C/min heating step from 30°C to 120°C was performed for all the polymers to reset the polymer thermal history. (3) Hold at 120°C for 2 minutes. (4) A 10°C/min cooling step was performed from 120°C to –50°C (5) Hold at –50°C for 10 minutes. This was to make sure that the sample actually reached –50°C since the cooling unit was not great. (6) Heat at 10°C/min from –50°C to 120°C. This last heating cycle was reported in the main manuscript.

Solid State NMR characterization: Experiments were conducted on a Bruker Avance II spectrometer equipped with a 4 mm H/F XY DVT and 2.5 mm X/F/H MAS DVT probe. Variable temperature (cooling) was done using an externally connected BCU II unit. Samples were held for at least 15 minutes at each temperature before measurements were made. Sample preparation was done in an Argon-filled glovebox. The crosslinked polymer samples were cut into fine powders or tiny chunks and packed into either a 2.5 mm or 4 mm rotor. The 4 mm rotors were covered using Kel-F caps, which limited our accessible temperature range (–20°C to 40°C). Adamantane was used as an external reference for ^1H (1.87 ppm) and ^{13}C (higher frequency peak at 38.6 ppm), 1 M NaF in H_2O was used as an external fluorine reference (–120 ppm), and 1M LiCl in H_2O was used as the external ^7Li reference (0 ppm). 90° pulses were measured and reference measurements were made before each NMR session. ^{19}F spectra was collected using a spin-synchronized Hahn-echo pulse sequence to remove the background from the probe. Spin-lattice (T_1) relaxation measurements were performed using a saturation-recovery sequence. Spectral fittings were performed of the central peak and the spinning sideband manifold using dmfit software package.[42]

References

1. Amanchukwu, C. V. The Electrolyte Frontier: A Manifesto. *Joule* **4**, 281–285 (2020).

2. Lin, D., Liu, Y. & Cui, Y. Reviving the lithium metal anode for high-energy batteries. *Nat. Nanotechnol. |* **12**, (2017).

3. Kerman, K., Luntz, A., Viswanathan, V., Chiang, Y.-M. & Chen, Z. Review—Practical Challenges Hindering the Development of Solid State Li Ion Batteries. *J. Electrochem. Soc.* **164**, A1731–A1744 (2017).

4. Randau, S. *et al.* Benchmarking the performance of all-solid-state lithium batteries. *Nat. Energy* doi:10.1038/s41560-020-0565-1

5. Janek, J. & Zeier, W. G. A solid future for battery development. (2016). doi:10.1038/NENERGY.2016.141

6. Marbella, L. E. *et al.* 7Li NMR Chemical Shift Imaging To Detect Microstructural Growth of Lithium in All-Solid-State Batteries. *Chem. Mater.* **31**, 2762–2769 (2019).

7. Kato, Y. *et al.* High-power all-solid-state batteries using sulfide superionic conductors. (2016). doi:10.1038/NENERGY.2016.30

8. Tan, D. H. S., Banerjee, A., Chen, Z. & Meng, Y. S. From nanoscale interface characterization to sustainable energy storage using all-solid-state batteries. *Nat. Nanotechnol. |* **15**, (2020).

9. Dixit, M. B. *et al.* Nanoscale Mapping of Extrinsic Interfaces in Hybrid Solid Electrolytes. *Joule* **4**, 207–221 (2020).

10. Manthiram, A., Yu, X. & Wang, S. Lithium battery chemistries enabled by solid-state electrolytes. (2017). doi:10.1038/natrevmats.2016.103

11. Gupta, A. & Sakamoto, J. Controlling Ionic Transport through the PEO-LiTFSI/LLZTO Interface. *Electrochem. Soc. Interface* **28**, 63–69 (2019).

12. Zheng, J., Wang, P., Liu, H. & Hu, Y.-Y. Interface-Enabled Ion Conduction in Li 10 GeP 2 S 12 −Poly(ethylene Oxide) Hybrid Electrolytes. (2019). doi:10.1021/acsaem.8b02008

13. Lopez, J., Mackanic, D. G., Cui, Y. & Bao, Z. Designing polymers for advanced battery chemistries. *Nat. Rev. Mater.* **4**, 312–330 (2019).

14. Amanchukwu, C. V, Harding, J. R., Shao-Horn, Y. & Hammond, P. T. Understanding the Chemical Stability of Polymers for Lithium−Air Batteries. *Chem. Mater* **27**, 550–561 (2014).

15. Harding, J. R., Amanchukwu, C. V, Hammond, P. T. & Shao-Horn, Y. Instability of Poly(ethylene oxide) upon Oxidation in Lithium−Air Batteries. *J. Phys. Chem. C* **119**, 6947–6955 (2015).

16. Strauss, E., Menkin, & S. & Golodnitsky, & D. On the way to high-conductivity single lithium-ion conductors. doi:10.1007/s10008-017-3638-8

17. Xue, Z., He, D. & Xie, X. Poly(ethylene oxide)-based electrolytes for lithium-ion batteries. *J. Mater. Chem. A* **3**, 19218–19253 (2015).

18. Pandian, S. *et al.* Electrochemical stability of ether based salt-in-polymer based electrolytes: Computational investigation of the effect of substitution and the type of salt. *J. Power Sources* **393**, 204–210 (2018).

19.   Xu, K. Nonaqueous liquid electrolytes for lithium-based rechargeable batteries. *Chem. Rev.* **104**, 4303–4417 (2004).

20.   Kimura, K., Motomatsu, J. & Tominaga, Y. Highly Concentrated Polycarbonate-Based Solid Polymer Electrolytes Having Extraordinary Electrochemical Stability. *J. Polym. Sci., Part B Polym. Phys* **54**, 2442–2447 (2016).

21.   Kimura, K., Yajima, M. & Tominaga, Y. A highly-concentrated poly(ethylene carbonate)-based electrolyte for all-solid-state Li battery working at room temperature. *Electrochem. commun.* **66**, 46–48 (2016).

22.   Sun, B. *et al.* Ion transport in polycarbonate based solid polymer electrolytes: experimental and computational investigations. *Phys. Chem. Chem. Phys* **18**, 9504 (2016).

23.   Amanchukwu, C. V *et al.* A New Class of Ionically Conducting Fluorinated Ether Electrolytes with High Electrochemical Stability. *J. Am. Chem. Soc* **142**, 7393–7403 (2020).

24.   Yu, Z. *et al.* Molecular design for electrolyte solvents enabling energy-dense and long-cycling lithium metal batteries. *Nat. Energy* **5**, 526–533 (2020).

25.   Ma, P., Mirmira, P. & Amanchukwu, C. V. Effect of Building Block Connectivity and Ion Solvation on Electrochemical Stability and Ionic Conductivity in Novel Fluoroether Electrolytes. *ACS Cent. Sci.* **7**, 1232–1244 (2021).

26.   Xu, H., Xie, J., Wang, J. & Deng, Y. Carbonyl-coordinating polymers for high-voltage solid-state lithium batteries: Solid polymer electrolytes. (2014). doi:10.1557/mre.2020.3

27.   Devaux, D. *et al.* Crosslinked perfluoropolyether solid electrolytes for lithium ion transport. *Solid State Ionics* **310**, 71–80 (2017).

28.   Wong, D. H. C. *et al.* Nonflammable perfluoropolyether-based electrolytes for lithium batteries. *Proc. Natl. Acad. Sci. U. S. A.* **111**, 3327–3331 (2014).

29.   Shah, D. B. *et al.* Effect of Anion Size on Conductivity and Transference Number of Perfluoroether Electrolytes with Lithium Salts. *J. Electrochem. Soc.* **164**, A3511–A3517 (2017).

30.   Diederichsen, K. M., McShane, E. J. & McCloskey, B. D. Promising Routes to a High Li + Transference Number Electrolyte for Lithium Ion Batteries. *ACS Energy Lett.* **2**, 2563–2575 (2017).

31.   Bouchet, R. *et al.* Single-ion BAB triblock copolymers as highly efficient electrolytes for lithium-metal batteries. *Nat. Mater.* **12**, 452–457 (2013).

32.   Abbrent, S. & Greenbaum, S. Recent progress in NMR spectroscopy of polymer electrolytes for lithium batteries. *Curr. Opin. Colloid Interface Sci.* **18**, 228–244 (2013).

33.   Chiappone, A., Jeremias, S., Bongiovanni, R. & Schönhoff, M. NMR study of photo-crosslinked solid polymer electrolytes: The influence of monofunctional oligoethers. *J. Polym. Sci. Part B Polym. Phys.* **51**, 1571–1580 (2013).

34.   Hayamizu, K., Aihara, Y. & Price, W. S. NMR and ion conductivity studies on cross-linked poly(ethyleneoxide-propyleneoxide) and branched polyether doped with LiN(SO2CF3)2. *Electrochim. Acta* **46**, 1475–1485 (2001).

35.   Every, H. A., Zhou, F., Forsyth, M. & Macfarlane, D. R. Lithium ion mobility in poly(vinyl alcohol) based polymer electrolytes as determined by 7 Li NMR spectroscopy. *Electrochim. Acta* **43**, 1465–1469 (1998).

36. Hayamizu, K., Aihara, Y. & Price, W. S. Correlating the NMR self-diffusion and relaxation measurements with ionic conductivity in polymer electrolytes composed of cross-linked poly„ethylene oxide-propylene oxide) doped with LiN„SO2CF3…2. *J. Chem. Phys* **113**, 4785 (2000).

37. Wong, D. H. C. *et al.* Phase Behavior and Electrochemical Characterization of Blends of Perfluoropolyether, Poly(ethylene glycol), and a Lithium Salt. *Chem. Mater.* **27**, 597−603 (2015).

38. Chen, X. C. *et al.* Study of segmental dynamics and ion transport in polymer-ceramic composite electrolytes by quasi-elastic neutron scattering †. *Mol. Syst. Des. Eng* **4**, 379 (2019).

39. Tchistiokov, A., Fontana, S. & Tonelli, C. Spearation of bifunctional perfluoropolyethers (PFPEs) having -CH2OH termination from their mixtures with - CH2OH monofunctional PFPEs. (2006).

40. Chung, S. H., Jeffrey, K. R. & Stevens, J. R. A 7Li nuclear magnetic resonance study of LiCF3SO3 complexed in poly(propylene-glycol). *J. Chem. Phys* **94**, 1803 (1991).

41. Chung, S. H., Wang, Y., Greenbaum, S. G., Golodnitsky, D. & Peled, E. Uniaxial stress effects in poly(ethylene oxide)-LiI polymer electrolyte film. A 7Li nuclear magnetic resonance study. *Electrochem. Solid-State Lett.* **2**, 553–555 (1999).

42. Massiot, D. *et al.* Modelling one- and two-dimensional solid-state NMR spectra. *Magn. Reson. Chem.* **40**, 70–76 (2002).

43. Maricq, M. M. & Waugh, J. S. NMR in rotating solids. *J. Chem. Phys.* **70**, 3300–3316 (1979).

44. Holmes, L. *et al.* Variable-temperature 17O NMR study of oxygen motion in the anionic conductor Bi26Mo10O69. *Chem. Mater.* **20**, 3638–3648 (2008).

45. Dunstan, M. T., Griffin, J. M., Blanc, F., Leskes, M. & Grey, C. P. Ion Dynamics in Li2CO3 Studied by Solid-State NMR and First-Principles Calculations. *J. Phys. Chem. C* **119**, 24255–24264 (2015).

46. Thrippleton, M. J., Cutajar, M. & Wimperis, S. Magic angle spinning (MAS) NMR linewidths in the presence of solid-state dynamics. *Chem. Phys. Lett.* **452**, 233–238 (2008).

47. Peng, J. *et al.* A Nuclear Magnetic Resonance Study of Cation and Anion Dynamics in Polymer−Ceramic Composite Solid Electrolytes. *ACS Appl. Polym. Mater* **2020**, 1180–1189 (2020).

48. Hopkins, B. J., Shao-Horn, Y. & Hart, D. P. *Suppressing corrosion in primary aluminum-air batteries via oil displacement*.

49. Lin, C.-L. L., Kao, H.-M. M., Wu, R.-R. R. & Kuo, P.-L. L. Multinuclear solid-state NMR, DSC, and conductivity studies of solid polymer electrolytes based on polyurethane/poly(dimethylsiloxane) segmented copolymers. *Macromolecules* **35**, 3083–3096 (2002).

50. Panero, S., Scrosati, B. & Greenbaum, S. G. Ionic conductivity and 7Li NMR Study of Poly(ethylene glycol) complexed with lithium salts. *Electrochim. Acta* **37**, 1533–1539 (1992).

51. Meziane, R., Bonnet, J.-P., Courty, M., Djellab, K. & Armand, M. Single-ion polymer electrolytes based on a delocalized polyanion for lithium batteries. *Electrochim. Acta* **57**, 14–19 (2011).